

Dynamical dark energy in light of cosmic distance measurements I: a demonstration using simulated datasets

Gan Gu^{1,2}, Xiaoma Wang^{1,2}, Xiaoyong Mu^{1,2}, Shuo Yuan¹, Gong-Bo Zhao^{1,2,3}

¹ National Astronomical Observatories, Chinese Academy of Sciences, Beijing, 100101, P.R.China, China; *gbzhao@nao.cas.cn*

² University of Chinese Academy of Sciences, Beijing, 100049, P.R.China

³ Institute for Frontiers in Astronomy and Astrophysics, Beijing Normal University, Beijing, 102206, P.R.China

Received 2024 Month Day; accepted 2024 Month Day

Abstract We develop methods to extract key dark energy information from cosmic distance measurements including the BAO scales and supernovae luminosity distances. Demonstrated using simulated datasets of the complete DESI, LSST and Roman surveys designed for BAO and SNe distance measurements, we show that using our method, the dynamical behaviour of the energy, pressure, equation of state (with its time derivative) of dark energy and the cosmic deceleration function can all be accurately recovered from high-quality data, which allows for robust diagnostic tests for dark energy models.

Key words: Cosmic Expansion History — Large-scale-structure — Baryon Acoustic Oscillations; Type Ia supernova

1 INTRODUCTION

The physical origin of the accelerating expansion of the Universe, which was discovered using observations of type Ia supernovae in 1998 (Riess et al. 1998; Perlmutter et al. 1999), remains unknown. Possible mechanisms for the cosmic acceleration include dark energy (Copeland et al. 2006), which is a dominating component of the cosmic energy budget today with a negative pressure, and modified gravity (Clifton et al.

2012), a framework in which Einstein’s general relativity (GR) gets modified. In both scenarios, an effective equation of state of dark energy, w , defined as a ratio of the pressure P over energy density ρ of the effective dark fluid, is a critical quantity for investigating models that can explain the cosmic acceleration. For example, $w = -1$ may mean that dark energy is essentially the vacuum energy, while an evolving w with cosmic time may suggest the dynamical nature of dark energy, or a breakdown of GR on cosmic scales. Therefore a direct reconstruction of w as a function of the scale factor a (or redshift z) from observations is of general interest (Sahni & Starobinsky 2006; Holsclaw et al. 2010; Clarkson & Zunckel 2010; Seikel et al. 2012; Crittenden et al. 2012; Zhao et al. 2012, 2017).

However, a reconstruction of $w(a)$ is not straightforward. Parametric reconstructions are easier to perform given the small number of free parameters to be determined, but the resultant reconstruction may be biased as it can only take the functional form assumed in the first place, which may not be appropriate. Non-parametric reconstructions are more general, but given the large number of degrees of freedom in the process, various kinds of datasets, such as the cosmic microwave background (CMB) (Spergel et al. 2003; Aghanim et al. 2020), type Ia supernovae (SNe Ia) (Riess et al. 1998; Perlmutter et al. 1999), baryonic acoustic oscillations (BAO) (Eisenstein & Hu 1998; Eisenstein et al. 2005; Cole et al. 2005; Alam et al. 2021) and redshift space distortions (RSD) (Kaiser 1987; Peacock et al. 2001; Alam et al. 2021), are combined for the purpose of degeneracy breaking. If one or more kinds of datasets are contaminated by unknown systematics, which is not impossible, the final reconstructed $w(a)$ inherits the systematics. In this sense, it is better to learn $w(a)$ from each individual type of datasets, and cross check the consistency, especially when datasets are in tension. But unfortunately this is difficult for non-parametric reconstruction methods.

Actually, one can learn important features of $w(a)$ without a direction reconstruction. In this work, we derive useful diagnostic quantities for $w(a)$ from cosmic distance measurements including the BAO scales and SN Ia luminosity distances, and validate our tests using simulated datasets including the galaxy survey of Dark Energy Spectroscopic Instrument (DESI) (Aghamousa et al. 2016) and SNe Ia surveys of Rubin Observatory’s Legacy Survey of Space and Time (LSST) (LSST Science Collaboration et al. 2009) and the Roman Space Telescope (Spergel et al. 2015).

This paper is structured as follows. We develop the methodology in Sec. 2, describe the simulated datasets in Sec. 3, and present the main result in Sec. 4, before conclude in Sec. 5. Some technical details are included in the Appendices.

2 FEATURES OF DARK ENERGY HIDDEN IN DISTANCE MEASUREMENTS

In this section, we show the information content of cosmic distance measurements that is relevant for dark energy studies, and propose methods to extract this piece of crucial information.

2.1 The shape function of dark energy

In a spatially flat Universe, the Hubble expansion rate $H(a)$ is related to the fractional dark energy density $X(a)$ through

$$f(a) \equiv AH^2a^3 = B [X(a)a^3] + C, \quad (1)$$

where A , B and C are constants. For example, for BAO observables, $A = r_d^2$, $B = r_d^2 H_0^2 (1 - \Omega_M)$, $C = r_d^2 H_0^2 \Omega_M$ with H_0 , r_d and Ω_M being the Hubble constant, the sound horizon at decoupling, and the present-day fractional matter density, respectively. The quantity $X(a)$ is defined as,

$$X(a) \equiv \frac{\rho_{\text{DE}}(a)}{\rho_{\text{DE}}(a=1)} = \exp \left[-3 \int_1^a \frac{1+w(y)}{y} dy \right], \quad (2)$$

where ρ_{DE} and w are the mean energy density, and the equation of state of dark energy, respectively.

From Eq. (1), it is clear that functions H^2a^3 and Xa^3 have the same shape, meaning that they are identical after a proper shift and normalisation. For example,

$$S[AH^2a^3] = S[Xa^3]; \quad S[f(a)] \equiv \frac{f(a) - f(a_*)}{f'(a_*)}, \quad (3)$$

where $S[f(a)]$ defines a shape function of $f(a)$, and a_* is a reference scale factor. Throughout the paper, the superscript $'$ denotes a derivative with respect to the scale factor a . Although the choice of a_* is arbitrary, it makes sense to choose one so that $f'(a_*)$ can be well measured, thus we can get a decent estimation for S and other quantities that depend on $f'(a_*)$. For the simulated datasets used in this work, we find that $a_* = 2/3$ is a reasonable choice to yield a tight constraint of $f'(a_*)$ using either the BAO or SNE datasets, so we set $a_* = 2/3$ for all results in this paper. We can obtain the shape information of Xa^3 through $S[AH^2a^3]$, which is a direct observable, and can be used as a diagnostic for dark energy models. For example,

$$\Lambda\text{CDM} \implies S[AH^2a^3] = \frac{a^3 - a_*^3}{3a_*^2}. \quad (4)$$

2.2 The pressure of dark energy

Since the pressure P of dark energy is proportional to wX , it follows that

$$R(a, a_*) \equiv \frac{P(a)}{P(a_*)} = \frac{w(a)X(a)}{w(a_*)X(a_*)} = \frac{a_*^2}{a^2} \frac{f'(a)}{f'(a_*)} \quad (5)$$

where a_* denotes a reference point for a normalization. From the definition, it is clear that,

$$\begin{aligned} w = -1 &\implies R = 1, \\ w = \text{constant} &\implies R = \left(\frac{a}{a_*}\right)^{-3(1+w)} \implies \frac{\log R}{\log(a/a_*)} = \text{constant} \end{aligned} \quad (6)$$

2.3 The characterisation function of dark energy

To obtain further information of $w(a)$, we take second derivative of $f(a)$ with respect to a and compare it to $f'(a)$ ¹. Specifically,

$$g(a) \equiv -\frac{1}{3} \left[a \frac{f''(a)}{f'(a)} + 1 \right] = w - \frac{a}{3} \frac{w'}{w}. \quad (7)$$

This function is a direct observable from distance measurements (Sahni et al. 2003; Alam et al. 2003), and it contains only w and w' . This means that it is free from degeneracies with any other cosmological parameters such as Ω_M, H_0 , etc. From the definition of $g(a)$, we see that,

$$\begin{aligned} w = -1 &\implies g = -1, \\ w = \text{constant} &\implies g = w = \text{constant}, \\ \text{At high redshifts} &\implies g \simeq w, \\ w \text{ slowly varies with time} &\implies g \simeq w, \\ w = w_0 + w_a(1 - a) &\implies g \text{ is close to a linear function of } a. \end{aligned} \quad (8)$$

These features can be used as diagnostics for dark energy models. For example, $g \neq -1$ rules out the Λ CDM model, and a varying g with time rules out the w CDM model (the model in which w is a constant). Furthermore, given a measurement of $g(a)$, we can obtain a relation between w and w' at any redshifts. This can in principle be used to differentiate dark energy models in the $w - w'$ phase-space (Caldwell & Linder 2005; Scherrer 2006; Chiba 2006), which is presented in a companion paper (Wang et al. 2024).

2.4 The deceleration function

The deceleration function $q(a)$ is another useful quantity that can be derived from $f(a)$, although it is not solely depends on dark energy parameters. Specifically,

$$q(a) \equiv -a \frac{H'}{H} - 1 = \frac{1}{2} \left[1 - \frac{af'(a)}{f(a)} \right]. \quad (9)$$

¹ An explicit derivation is included in Sec. A.

2.5 The parametrisation of the cosmic distances

All the above-mentioned useful functions can be derived from $f(a)$, thus it is important to derive $f(a)$ from distance measurements in an efficient and accurate way. Following Zhu et al. (2015), we parametrise the cosmological distances in form of,

$$\frac{D_A(a)}{D_{A,\text{fid}}(a)} = \alpha_0 \left(1 + \alpha_1 x + \frac{1}{2} \alpha_2 x^2 + \frac{1}{6} \alpha_3 x^3 + \frac{1}{24} \alpha_4 x^4 + \frac{1}{120} \alpha_5 x^5 + \frac{1}{720} \alpha_6 x^6 \right),$$

$$x \equiv \frac{\chi_{\text{fid}}(a)}{\chi_{\text{fid}}(a_p)} - 1, \quad (10)$$

where a_p is the pivot point for the expansion, and we choose to set $a_p = 2/3$ in this work. As demonstrated in Sec. B.1, the choice of a_p has almost no impact on the final reconstruction result. Since Eq. (10) is essentially a Taylor expansion, we need a criterion to determine the maximal order of expansion to be included in the series. Keeping more terms in the expansion makes this parametric reconstruction more accurate, but this also inflates the uncertainties due to the degeneracies among parameters. Therefore a balance between the reconstruction bias and the statistical uncertainties is required when determining the highest order of the expansion. Note that this depends on the dataset being used - better measured data can help to constrain more parameters. Given the sensitivity of DESI, LSST and Roman, we find that keeping α_0 to α_6 terms in the expansion is a sensible choice when all datasets are combined² for the four fiducial dark energy models considered in this work (see a demonstration in Sec. B.2), which cover a wide range of phenomenological dark energy models.

The subscript ‘fid’ stands for the fiducial cosmology, which is chosen to be a Λ CDM model favored by the latest Planck observations (Planck Collaboration et al. 2020). Using the relation between H and D_A in a flat Universe, we find that,

$$\frac{H_{\text{fid}}(a)}{H(a)} = \beta_0 (1 + \beta_1 x + \beta_2 x^2 + \beta_3 x^3 + \beta_4 x^4 + \beta_5 x^5 + \beta_6 x^6), \quad (11)$$

where parameters β_i can be derived from α_i , and an explicit derivation is included in Appendix C. Equations (10) and (11) allow for a parametric reconstruction of $f(a)$ from distance measurements³, including the BAO distance measurements⁴, the luminosity distance measurements from SN Ia observations, and $H(z)$ measurements from the cosmic chronometers (Stern et al. 2010).

² For the case of BAO alone, we keep α_0 to α_4 terms to avoid overfitting.

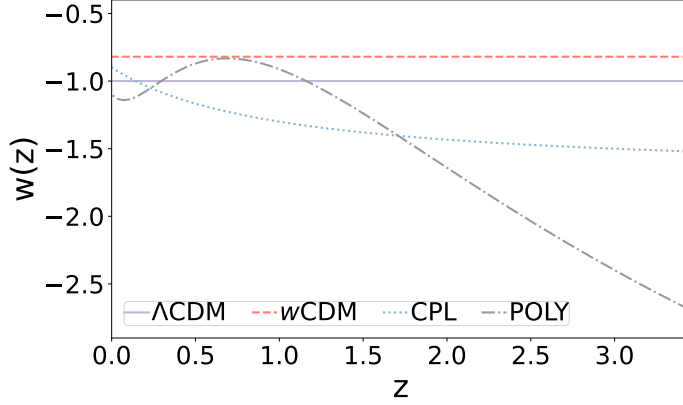
³ Note that when fitting α 's in Eqs. (10) and (11) to distance measurements, the derived X may not be positive-definite. Therefore when deriving quantities related to f' including the pressure function and the g function, we apply a prior of $X > 0$. We check the posteriors and find that this has a marginal effect on the final result.

⁴ Note that galaxy surveys provide BAO distance measurements of D_A/r_d , Hr_d or D_V/r_d , instead of D_A , H or D_V , but this does not matter since the unknown amplitude r_d can be absorbed into α_0 or β_0 . As we only use the shape information of $f(a)$ for dark energy studies, the value of α_0 or β_0 is actually irrelevant.

Dark energy models	$w(a)$
Λ CDM	$w = -1$
w CDM	$w = -0.82$
CPL	$w = -0.9 - 0.8(1 - a)$
POLY	$w = -1.1 - 1.3(1 - a) + 11.2(1 - a)^2 - 15.7(1 - a)^3$

Table 1: Dark energy models used for producing the mock datasets.

3 SIMULATED DATASETS AND PARAMETER ESTIMATION

Fig. 1: The $w(z)$ models used as fiducial models in this work.

In this section, we present the simulated datasets used for this work, including the mock BAO datasets for the complete DESI survey, and the mock SNe Ia datasets assuming a sensitivity of the LSST and Roman surveys.

To start with, we choose four phenomenological dark energy models as fiducial models shown in Table 1 and Fig. 1. These include the Λ CDM model ($w = -1$), a w CDM model with $w = -0.82$, a Chevallier-Polarski-Linder (CPL) model (Chevallier & Polarski 2001; Linder 2003) with $w_0 = -0.9$ and $w_a = -0.8$, and a more complicated model of $w(a)$, which is a polynomial of $(1 - a)$ (POLY). To be generic, the parameters for the CPL and POLY models are chosen so that $w(a)$ is allowed to cross the $w = -1$ boundary, as motivated by observations (Feng et al. 2005; Zhao et al. 2012, 2017; Wang et al. 2018; Adame et al. 2024). Throughout the paper we assume fiducial values of $\Omega_M = 0.315$ and $H_0 = 67.4 \text{ km s}^{-1} \text{ Mpc}^{-1}$, which are consistent with values in a Λ CDM model favored by Planck observations (Aghanim et al. 2020). Given the input dark energy models and fiducial values of Ω_M and H_0 , the simulated BAO and SNe Ia observables, including the mean values and data covariance matrix, can be created, if the sensitivity of the relevant surveys is assumed.

3.1 Simulated BAO observables

For the BAO observables, we assume a sensitivity of the complete DESI survey. DESI is a Stage IV ground-based galaxy spectroscopic survey, measuring the expansion rate and the growth rate of cosmic structures at (sub)percent level across a wide range of redshifts. We follow the official DESI specifications (DESI Collaboration et al. 2023), and use the forecast sensitivity of D_A/r_d and Hr_d derived from tracers including the Bright Galaxy Samples (BGS), Luminous Red Galaxies (LRGs), Emission Line Galaxies (ELGs), Quasars (QSOs) and the Lyman- α forest ($\text{Ly}\alpha$) at $0 < z < 3.5$.

3.2 Simulated SNe Ia observables

Type Ia supernovae, as cosmic standard candles, offer measurements of luminosity distances at multiple redshifts. LSST (LSST Science Collaboration et al. 2009) and Roman (Spergel et al. 2015) are two main forthcoming SNe Ia surveys with complementary redshift coverage, namely, LSST aims to observe hundreds of thousands SNe at low and intermediate redshifts, while Roman is expected to detect SNe up to $z = 3$. We assume that the uncertainties of the SNe distance modulus are quadratic sums of the intrinsic scatter of $\sigma_{\text{int}} = 0.13$ mag and both the lensing-induced scatter and the peculiar velocity scatter⁵. For the expected number of SNe to be detected by LSST, we follow Matos et al. (2023) to assume a 10-year survey over $18,000 \text{ deg}^2$ with a 15% completeness at $z < 0.7$, and for Roman, we assume a WIDE survey mode (Rose et al. 2021).

3.3 Parameter estimation

Given the simulated datasets, which include a data vector storing the mean value of the observables, and a data covariance matrix, we perform a Monte Carlo Markov Chain (MCMC) analysis to constrain the α parameters defined in Eq. (10) using the `Cobaya` software (Torrado & Lewis 2021).

4 RESULTS

In this section, we present the main result of this work, as summarised in Figs. 2-5.

Fig. 2 shows the reconstructed shape function of Xa^3 , derived from the simulated DESI BAO data alone (top panels) and from the simulated DESI BAO + LSST (SNe) + Roman (SNe) (middle panels). For a better visualisation, we show the result normalised by S predicted by the Λ CDM model in the bottom panel. As shown, the input models (shown in dashed blue curves) are well recovered in all cases, validating our pipeline for reconstructing $S[Xa^3]$ from data. We find that forthcoming BAO combined with SNe

⁵ We assume ideal cases with no systematics in this simulation.

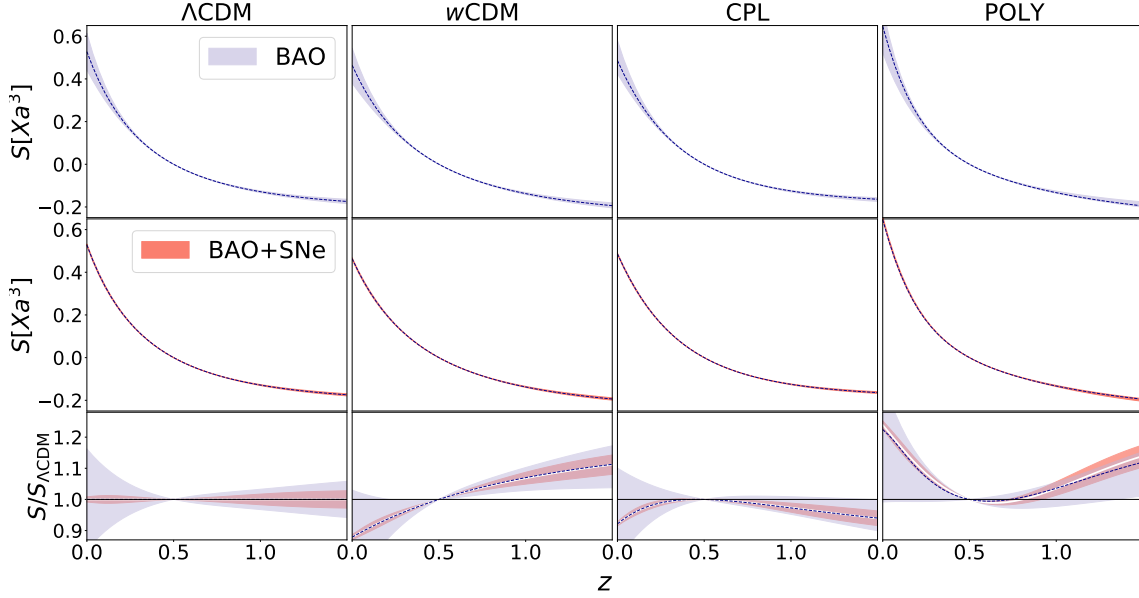


Fig. 2: The reconstructed shape function of dark energy, $S[Xa^3]$, as a function of redshift z for four input $w(z)$ models as illustrated in the legend. In all panels, the blue dashed lines denote the input model, and the shaded bands show the 68% confidence level (CL) reconstruction. The top and middle panels present results derived from the simulated BAO assuming a complete DESI survey (blue bands) and BAO combined with SNe datasets assuming complete LSST and Roman surveys (red bands), respectively. The bottom panel shows the result normalised by the Λ CDM model $S_{\Lambda\text{CDM}}$. The white curves in the middle show the mean of the reconstructed S function.

observations can well constrain the shape function of dark energy, making it possible to use this function to test the Λ CDM model to a high precision.

Figs. 3 - 5 show the reconstructed pressure function $P(z)$ of dark energy (normalised by the value of P at a_*), the characterisation function $g(z)$, and the deceleration function $q(z)$, respectively. As shown, all input models can be recovered at $z \gtrsim 0.1$ within the small uncertainties derived from the simulated datasets of BAO (DESI) + SNe (LSST+Roman). The POLY model is less well reproduced at $z \lesssim 0.1$ due to its wiggly feature at such low redshifts, which requires higher-order terms in the expansion in Eq. (10). We have tried an expansion of Eq. (10) with the α_7 term (see Sec. B.2), which indeed improves the accuracy of the reconstruction, but with much larger uncertainties. Therefore our default choice (keeping up to the α_6 term) is a reasonable compromise.

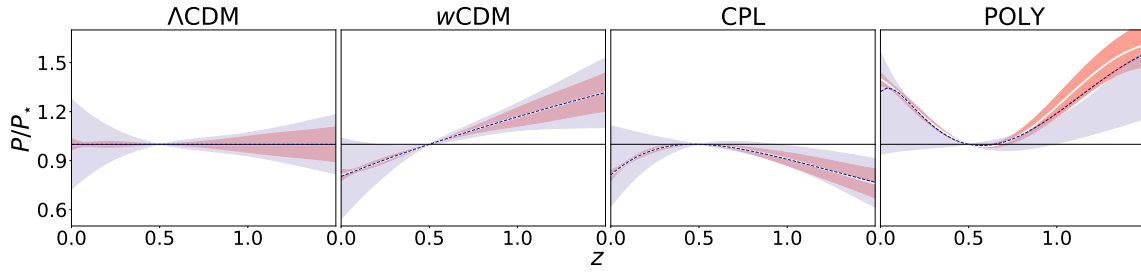


Fig. 3: The reconstructed pressure function of dark energy, normalised at $a = a_*$, as a function of redshift z for four input $w(z)$ models as illustrated in the legend. In all panels, the blue dashed lines denote the input model, and the shaded bands show the 68% confidence level (CL) reconstruction derived from the simulated BAO (blue bands) and BAO combined with SNe datasets (red bands), respectively. The horizontal black lines show the Λ CDM prediction of $P/P_* = 1$ for a reference.

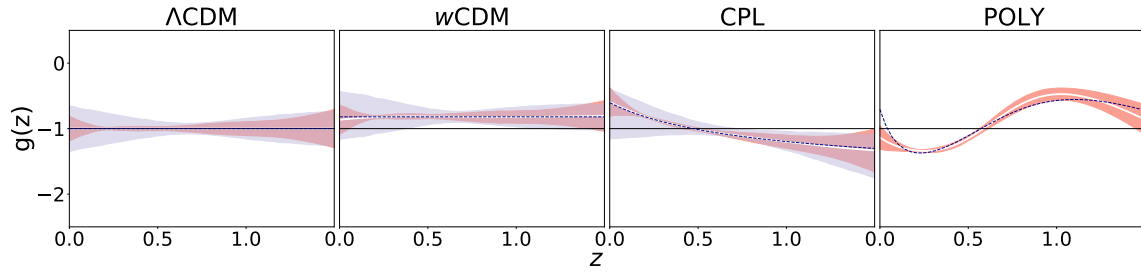


Fig. 4: Same as Fig. 3, but for $g(z)$. The horizontal black lines show the Λ CDM prediction of $g = -1$ for a reference.

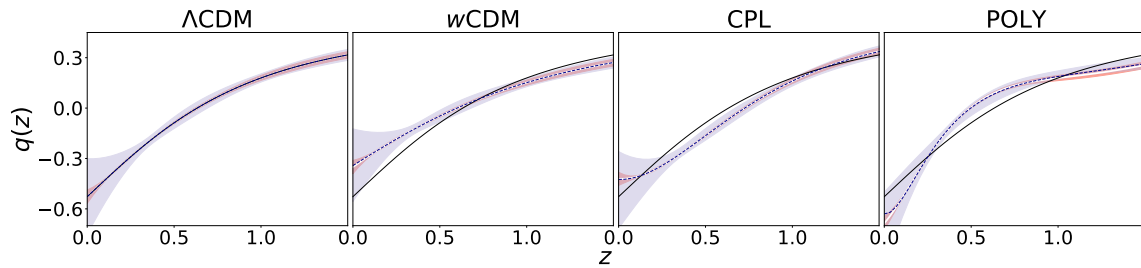


Fig. 5: Same as Fig. 4, but for the deceleration function $q(z)$. The black lines show the Λ CDM prediction for a reference.

5 CONCLUSION AND DISCUSSIONS

In this era of precision cosmology, we have been gaining access to high quality observational data probing the Universe from various angles, which is deepening our understanding of the cosmos. Revealing the nature of dark energy is one of the most challenging problems to tackle in modern cosmology. As dark energy is

the driving force of the current acceleration of the spacetime expansion, it is crucial to develop methods and tools to capture critical features of dark energy from measurements of the cosmic expansion.

In this work, we develop methods to extract important features of dark energy, including the shape function of the energy of dark energy $S[Xa^3]$, the evolution history of the pressure $P(a)/P(a_*)$, the characterisation function $g(a)$, and the deceleration function $q(a)$, from cosmic distance measurements, primarily including BAO and SNe measurements. We apply our pipeline to simulated DESI, LSST and Roman datasets created for a range of phenomenological dark energy models, and find that our method can well capture the dynamical features of dark energy hidden in the simulated datasets. As our method only extracts information of dark energy from distance measurements, it is by design free from degeneracies among other cosmological parameters. This allows for diagnostic dark energy tests using individual type of observational data, which is important for dark energy studies.

Our method is directly applicable to existing cosmic distance measurements for dark energy tests, which is released in a companion paper (Wang et al. 2024).

6 ACKNOWLEDGMENTS

We thank Ruiyang Zhao for helpful discussions. All authors are supported by the National Key R & D Program of China (2023YFA1607800, 2023YFA1607803), NSFC grants (No. 11925303 and 11890691), and by a CAS Project for Young Scientists in Basic Research (No. YSBR-092). SY is also supported by a NSFC grant (No. 12203062). SY and GBZ are also supported by science research grants from the China Manned Space Project with No. CMS-CSST-2021-B01. GBZ is also supported by the New Cornerstone Science Foundation through the XPLOER prize.

Appendix A: DERIVATION OF THE CHARACTERISATION FUNCTION

By definition,

$$f(a) \equiv H^2 a^3 = H_0^2 [\Omega_M + (1 - \Omega_M)X(a)a^3], \quad (\text{A.1})$$

Then

$$f'(a) = \frac{d}{da} H_0^2 [\Omega_M + (1 - \Omega_M)X(a)a^3] = -3H_0^2(1 - \Omega_M)w(a)X(a)a^2, \quad (\text{A.2})$$

$$\begin{aligned} f''(a) &= -3H_0^2(1 - \Omega_M) \frac{d}{da} [w(a)X(a)a^2] \\ &= -3H_0^2(1 - \Omega_M) \left[w'(a)X(a)a^2 + w(a)X(a)(-3)\frac{1+w(a)}{a}a^2 + w(a)X(a)2a \right] \\ &= -3H_0^2(1 - \Omega_M) [a^2 w'(a)X(a) - aw(a)X(a) - 3aw^2(a)X(a)], \end{aligned} \quad (\text{A.3})$$

Thus

$$\frac{f''(a)}{f'(a)} = \frac{1}{a} \left[a \frac{w'(a)}{w(a)} - 3w(a) - 1 \right]. \quad (\text{A.4})$$

Hence,

$$g(a) \equiv w - \frac{a w'}{3 w} = -\frac{1}{3} \left[a \frac{f''(a)}{f'(a)} + 1 \right]. \quad (\text{A.5})$$

Appendix B: CHOICE OF THE PIVOT POINT AND ORDER OF THE EXPANSION

B.1. Impact of the choice of z_p on the reconstructed f

We test how the choice of z_p affects the reconstructed dark energy shape function f , as defined in Eq. (3). For this test, we reconstruct f from the simulated DESI data created with various dark energy models with four choices of z_p of 0.2, 0.4, 0.6 and 0.8, and show the result in Fig. B.1. As expected, the choice of z_p has negligible effect on the final reconstructed f , which demonstrates the robustness of our reconstruction result.

B.2. Impact of the expansion order

The maximum order of the expansion in Eq. (10) does affect the final reconstruction of the functions that are closely related to dark energy. As a demonstration, in Fig. B.2 we show the reconstructed $g(a)$ from the simulated DESI+LSST+Roman datasets for the POLY model with different maximum orders of expansion, namely, we use expansions up to the x^5 ($O5$), x^6 ($O6$) and x^7 ($O7$) terms in Eq. (C.1), respectively. As shown, the reconstruction bias is significant in the $O5$ case, while the uncertainties are large in the $O7$ case, making the $O6$ case a reasonable compromise, which is used for producing main results of this work.

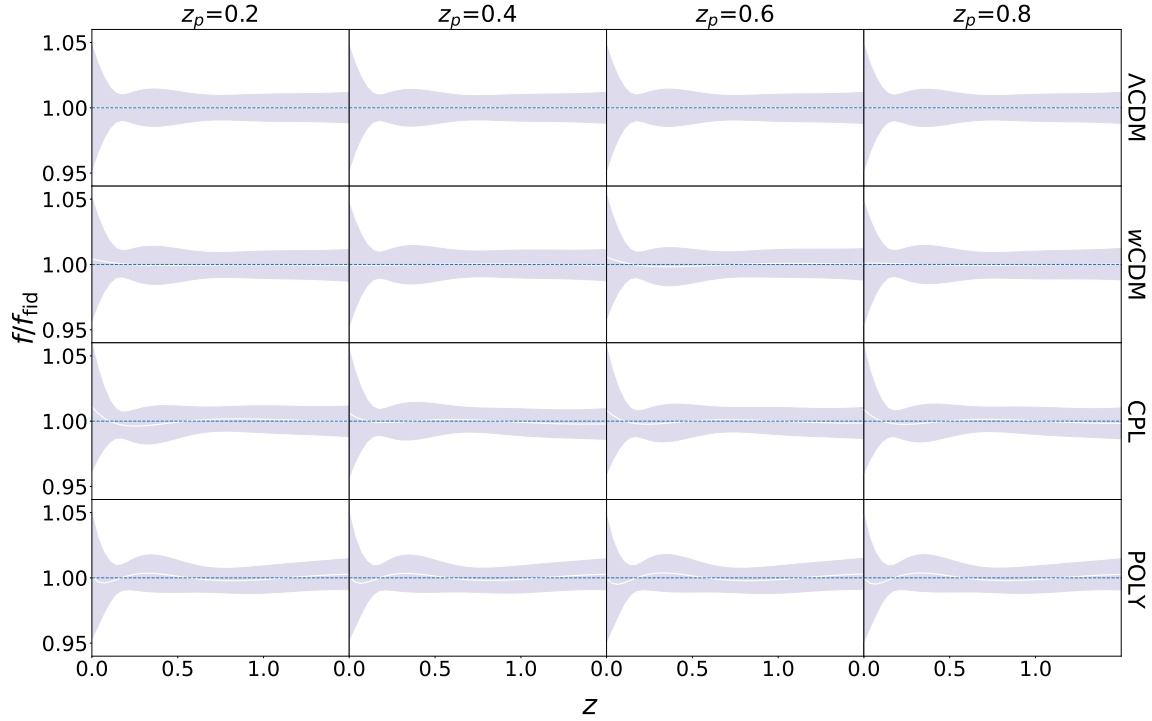


Fig. B.1: The reconstructed dark energy shape function f normalised by the input fiducial function for four different choices of z_p . The mean (white lines) and 68% CL uncertainties (shaded regions) derived from the simulated DESI data are shown for four phenomenological dark energy models illustrated in the legend. The horizon blue dashed lines show $f/f_{\text{fid}} = 1$ for a reference.

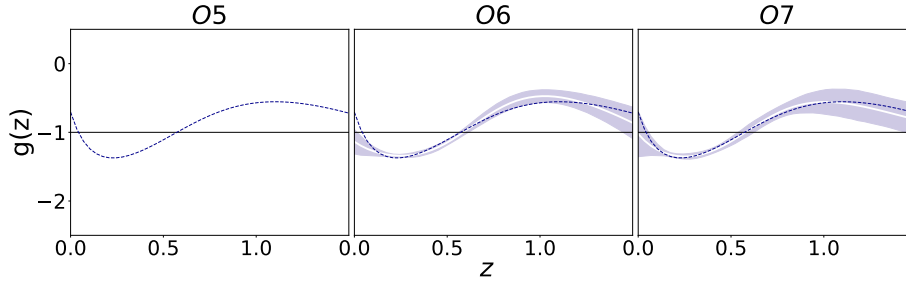


Fig. B.2: The mean (white lines) and 68% CL uncertainties (shaded regions) of the reconstructed g function of the POLY fiducial model using expansions up to the x^5 (O5), x^6 (O6) and x^7 (O7) terms in Eq. (C.1). The blue dashed lines show the input fiducial model, and the black horizon lines show the Λ CDM prediction for a reference.

Appendix C: DERIVATION OF THE DISTANCE-REDSHIFT PARAMETERS

To be general, we expand χ/χ_{fid} up to order N , namely,

$$\chi(z) = \alpha_0 \left(1 + \sum_{i=1}^N \frac{1}{i!} \alpha_i x^i \right) \chi_{\text{fid}}(z) \quad (\text{C.1})$$

where

$$x \equiv \chi_{\text{fid}}(z)/\chi_{\text{fid}}(z_p) - 1 \quad (\text{C.2})$$

Taking derivative of Eq. (C.1) with respect to z , we have

$$\begin{aligned} \frac{1}{H(z)} = \frac{d}{dz} \chi(z) &= \alpha_0 \left[\chi_{\text{fid}}(z) \left(\sum_{i=1}^N \frac{1}{(i-1)!} \alpha_i x^{i-1} \right) \frac{dx}{dz} + \left(1 + \sum_{i=1}^N \frac{1}{i!} \alpha_i x^i \right) \frac{d}{dz} \chi_{\text{fid}}(z) \right] \\ &= \alpha_0 \left[\chi_{\text{fid}}(z) \left(\sum_{i=1}^N \frac{1}{(i-1)!} \alpha_i x^{i-1} \right) \frac{1}{H_{\text{fid}}(z) \chi_{\text{fid}}(z_p)} + \left(1 + \sum_{i=1}^N \frac{1}{i!} \alpha_i x^i \right) \frac{1}{H_{\text{fid}}(z)} \right] \end{aligned} \quad (\text{C.3})$$

Then

$$\begin{aligned} \frac{H_{\text{fid}}(z)}{H(z)} &= \alpha_0 \left[\left(\sum_{i=1}^N \frac{1}{(i-1)!} \alpha_i x^{i-1} \right) \frac{\chi_{\text{fid}}(z)}{\chi_{\text{fid}}(z_p)} + \left(1 + \sum_{i=1}^N \frac{1}{i!} \alpha_i x^i \right) \right] \\ &= \alpha_0 \left[\left(\sum_{i=1}^N \frac{1}{(i-1)!} \alpha_i x^{i-1} \right) (1+x) + \left(1 + \sum_{i=1}^N \frac{1}{i!} \alpha_i x^i \right) \right] \end{aligned} \quad (\text{C.4})$$

For the case of $N = 6$ for example,

$$\frac{D_A}{D_{A,\text{fid}}} = \alpha_0 \left(1 + \alpha_1 x + \frac{1}{2} \alpha_2 x^2 + \frac{1}{6} \alpha_3 x^3 + \frac{1}{24} \alpha_4 x^4 + \frac{1}{120} \alpha_5 x^5 + \frac{1}{720} \alpha_6 x^6 \right) \quad (\text{C.5})$$

$$\begin{aligned} \frac{H_{\text{fid}}(z)}{H(z)} &= \alpha_0 \left(\alpha_1 + \alpha_2 x + \frac{1}{2} \alpha_3 x^2 + \frac{1}{6} \alpha_4 x^3 + \frac{1}{24} \alpha_5 x^4 + \frac{1}{120} \alpha_6 x^5 \right) (1+x) + \\ &\alpha_0 \left(1 + \alpha_1 x + \frac{1}{2} \alpha_2 x^2 + \frac{1}{6} \alpha_3 x^3 + \frac{1}{24} \alpha_4 x^4 + \frac{1}{120} \alpha_5 x^5 + \frac{1}{720} \alpha_6 x^6 \right) \end{aligned} \quad (\text{C.6})$$

References

- Adame, A. G., et al. 2024, arXiv:2404.03002 6
- Aghamousa, A., et al. 2016, arXiv:1611.00036 2
- Aghanim, N., et al. 2020, *Astron. Astrophys.*, 641, A6, [Erratum: *Astron. Astrophys.* 652, C4 (2021)] 2, 6
- Alam, S., et al. 2021, *Phys. Rev. D*, 103, 083533 2
- Alam, U., Sahni, V., Saini, T. D., & Starobinsky, A. A. 2003, *Mon. Not. Roy. Astron. Soc.*, 344, 1057 4
- Caldwell, R. R., & Linder, E. V. 2005, *Phys. Rev. Lett.*, 95, 141301 4
- Chevallier, M., & Polarski, D. 2001, *Int. J. Mod. Phys. D*, 10, 213 6
- Chiba, T. 2006, *Phys. Rev. D*, 73, 063501, [Erratum: *Phys. Rev. D* 80, 129901 (2009)] 4
- Clarkson, C., & Zunckel, C. 2010, *Phys. Rev. Lett.*, 104, 211301 2
- Clifton, T., Ferreira, P. G., Padilla, A., & Skordis, C. 2012, *Phys. Rept.*, 513, 1 1
- Cole, S., Percival, W. J., Peacock, J. A., et al. 2005, *Mon. Not. Roy. Astron. Soc.*, 362, 505 2
- Copeland, E. J., Sami, M., & Tsujikawa, S. 2006, *Int. J. Mod. Phys. D*, 15, 1753 1
- Crittenden, R. G., Zhao, G.-B., Pogosian, L., Samushia, L., & Zhang, X. 2012, *JCAP*, 02, 048 2
- DESI Collaboration, Adame, A. G., Aguilar, J., et al. 2023, arXiv e-prints, arXiv:2306.06307 7
- Eisenstein, D. J., & Hu, W. 1998, *Astrophys. J.*, 496, 605 2
- Eisenstein, D. J., Zehavi, I., Hogg, D. W., et al. 2005, *Astrophys. J.*, 633, 560 2
- Feng, B., Wang, X.-L., & Zhang, X.-M. 2005, *Phys. Lett. B*, 607, 35 6
- Holsclaw, T., Alam, U., Sanso, B., et al. 2010, *Phys. Rev. Lett.*, 105, 241302 2
- Kaiser, N. 1987, *Mon. Not. Roy. Astron. Soc.*, 227, 1 2
- Linder, E. V. 2003, *Phys. Rev. Lett.*, 90, 091301 6
- LSST Science Collaboration, Abell, P. A., Allison, J., et al. 2009, arXiv e-prints, arXiv:0912.0201 2, 7
- Matos, I. S., Quartin, M., Amendola, L., Kunz, M., & Sturani, R. 2023, arXiv e-prints, arXiv:2311.17176 7
- Peacock, J. A., et al. 2001, *Nature*, 410, 169 2
- Perlmutter, S., Aldering, G., Goldhaber, G., et al. 1999, *ApJ*, 517, 565 1, 2
- Planck Collaboration, Aghanim, N., Akrami, Y., et al. 2020, *A&A*, 641, A6 5
- Riess, A. G., Filippenko, A. V., Challis, P., et al. 1998, *AJ*, 116, 1009 1, 2
- Rose, B. M., et al. 2021, arXiv:2111.03081 7
- Sahni, V., Saini, T. D., Starobinsky, A. A., & Alam, U. 2003, *JETP Lett.*, 77, 201 4
- Sahni, V., & Starobinsky, A. 2006, *Int. J. Mod. Phys. D*, 15, 2105 2
- Scherrer, R. J. 2006, *Phys. Rev. D*, 73, 043502 4
- Seikel, M., Clarkson, C., & Smith, M. 2012, *JCAP*, 06, 036 2
- Spiegel, D. N., et al. 2003, *Astrophys. J. Suppl.*, 148, 175 2

- Spergel, D., Gehrels, N., Baltay, C., et al. 2015, arXiv e-prints, arXiv:1503.03757 2, 7
- Stern, D., Jimenez, R., Verde, L., Kamionkowski, M., & Stanford, S. A. 2010, JCAP, 02, 008 5
- Torrado, J., & Lewis, A. 2021, Journal of Cosmology and Astroparticle Physics, 2021, 057 7
- Wang, X., Gu, G., Mu, X., Yuan, S., & Zhao, G.-B. 2024, arXiv:2404.06310 4, 10
- Wang, Y., Pogosian, L., Zhao, G.-B., & Zucca, A. 2018, Astrophys. J. Lett., 869, L8 6
- Zhao, G.-B., Crittenden, R. G., Pogosian, L., & Zhang, X. 2012, Phys. Rev. Lett., 109, 171301 2, 6
- Zhao, G.-B., et al. 2017, Nature Astron., 1, 627 2, 6
- Zhu, F., Padmanabhan, N., & White, M. 2015, Monthly Notices of the Royal Astronomical Society, 451, 236–243 5